Multiparametric 3T Prostate Magnetic Resonance Imaging to Detect Cancer: Histopathological Correlation Using Prostatectomy Specimens Processed in Customized Magnetic Resonance Imaging Based Molds

Baris Turkbey, Haresh Mani, Vijay Shah,* Ardeshir R. Rastinehad, Marcelino Bernardo, Thomas Pohida, Yuxi Pang,† Dagane Daar, Compton Benjamin, Yolanda L. McKinney, Hari Trivedi, Celene Chua, Gennady Bratslavsky, Joanna H. Shih, W. Marston Linehan, Maria J. Merino, Peter L. Choyke and Peter A. Pinto‡

From the Molecular Imaging Program (BT, VS, MB, DD, YLM, PLC), Laboratory of Pathology (HM, MJM), Urologic Oncology Branch (ARR, CB, HT, CC, GB, WML, PAP) and Biometric Research Branch, Division of Cancer Treatment and Diagnosis (JHS), National Cancer Institute, National Institutes of Health, and Division of Computational Bioscience, Center for Information Technology, National Institutes of Health (TP), Bethesda, and Imaging Physics, SAIC Frederick, Inc., National Cancer Institute-Frederick, Frederick (VS, MB), Maryland, and Philips Healthcare, Cleveland, Ohio (YP)

Abbreviations and Acronyms

3D = 3-dimensional
A&CG = anterior horns of peripheral zone and central gland
ADC = apparent diffusion coefficient
CG = central gland
DCE = dynamic contrast enhanced
DW = diffusion weighted
GEE = generalized estimating equation
MRI = magnetic resonance imaging
MRS = magnetic resonance spectroscopy
NPV = negative predictive value
PPV = positive predictive value
PSA = prostate specific antigen
PZ = peripheral zone
T2W = T2-weighted
TRUS = transrectal ultrasound

Purpose: We determined the prostate cancer detection rate of multiparametric magnetic resonance imaging at 3T. Precise one-to-one histopathological correlation with magnetic resonance imaging was possible using prostate magnetic resonance imaging based custom printed specimen molds after radical prostatectomy.

Materials and Methods: This institutional review board approved prospective study included 45 patients (mean age 60.2 years, range 49 to 75) with a mean prostate specific antigen of 6.37 ng/ml (range 2.3 to 23.7) who had biopsy proven prostate cancer (mean Gleason score of 6.7, range 6 to 9). Before prostatectomy all patients underwent prostate magnetic resonance imaging using endorectal and surface coils on a 3T scanner, which included triplane T2-weighted magnetic resonance imaging, apparent diffusion coefficient maps of diffusion weighted magnetic resonance imaging, dynamic contrast enhanced magnetic resonance imaging and spectroscopy. The prostate specimen was whole mount sectioned in a customized mold, allowing geometric alignment to magnetic resonance imaging. Tumors were mapped on magnetic resonance imaging and histopathology. Sensitivity, specificity, positive predictive value and negative predictive value of magnetic resonance imaging for cancer detection were calculated. In addition, the effects of tumor size and Gleason score on the sensitivity of multiparametric magnetic resonance imaging were evaluated.

Submitted for publication March 21, 2011.
Study received institutional review board approval.
Supported by the Intramural Research Program of the National Institutes of Health, National Cancer Institute, Center for Cancer Research.
* Financial interest and/or other relationship with VirtualScopics.
† Financial interest and/or other relationship with Philips Healthcare.
‡ Correspondence: Urologic Oncology Branch, National Cancer Institute, 10 Center Dr., MSC 1210, Bldg 10, Room 2-5940, Bethesda, Maryland 20892-1088 (telephone: 301-496-6353; FAX: 301-402-0922; e-mail: pintop@mail.nih.gov).

See Editorial on page 1756.

For another article on a related topic see page 2101.

0022-5347/11/1865-1818/0
THE JOURNAL OF UROLOGY

Vol. 186, 1818-1824, November 2011
Printed in U.S.A.
DOI:10.1016/j.juro.2011.07.013

Results: The positive predictive value of multiparametric magnetic resonance imaging to detect prostate cancer was 98%, 98% and 100% in the overall prostate, peripheral zone and central gland, respectively. The sensitivity of magnetic resonance imaging sequences was higher for tumors larger than 5 mm in diameter as well as for those with higher Gleason scores (greater than 7, $p < 0.05$).

Conclusions: Prostate magnetic resonance imaging at 3T allows for the detection of prostate cancer. A multiparametric approach increases the predictive power of magnetic resonance imaging for diagnosis. In this study accurate correlation between multiparametric magnetic resonance imaging and histopathology was obtained by the patient specific, magnetic resonance imaging based mold technique.

Key Words: prostatic neoplasms, prostatectomy, magnetic resonance imaging, magnetic resonance spectroscopy, pathology

PROSTATE cancer is the most common cancer among American men with an estimated 217,730 new cases and 32,050 deaths in 2010.[1] Screening with PSA has led to increased detection of prostate cancer, and the detected cancers are smaller, lower grade and lower stage. Therefore, validating imaging methods for prostate cancer detection has become more challenging. MRI, including anatomical and functional sequences, has been shown to be effective in the preoperative detection and local staging of prostate cancer in various studies with different magnetic field strengths.[2–15] However, there are limitations in validating MRI findings even with whole mount histopathology as the gold standard because freehand slicing can easily result in deformation of the prostatectomy specimens, thereby altering the orientation of histological sections compared to MRI.[12,16,17] These mismatches between histopathology and MRI can make it difficult to assess the true accuracy of MRI. In this study we describe our experience using a customized specimen mold based on the data extracted from the preoperative MRI, which allows sectioning of the prostate in the same planes as the in vivo MRI slices. The findings of multiparametric MRI (T2W MRI, ADC maps of DW MRI, MRS, DCE MRI) were correlated with the resulting registered histopathology slices.

MATERIALS AND METHODS

Study Design and Population

This prospectively designed, single institution study was approved by the local institutional review board, and was compliant with the Health Insurance Portability and Accountability Act of 1996. Informed consent was obtained from each patient. A total of 45 consecutive patients were enrolled in the study between July 2008 and July 2009. Mean patient age was 60.2 years (median 60, range 49 to 75) and mean PSA was 6.37 ng/ml (median 5.8, range 2.3 to 23.7). All patients had biopsy proven adenocarcinoma of the prostate and mean Gleason score was 6.7 (median 7, range 6 to 9). The inclusion criteria required that robotic assisted radical prostatectomy be performed within 180 days of imaging without any intervening treatment. Exclusion criteria were contraindications to MRI (cardiac pacemakers, prosthetic valves, severe claustrophobia etc) or inability to have an endorectal coil placed (anorectal surgery, colostomy, inflammatory bowel disease, severe hemorrhoids etc).

Magnetic Resonance Imaging

All MRI studies were performed using a combination of an endorectal coil (BPX-30, Medrad, Pittsburgh, Pennsylvania) tuned to 127.8 MHz and a 16-channel cardiac coil (SENSE, Philips Medical Systems, Best, The Netherlands) on a 3T magnet (Achieva, Philips Medical Systems) without prior bowel preparation. The endorectal coil was inserted using a semi-anesthetic gel (lidocaine) while the patient was in left lateral decubitus position. The balloon surrounding the coil was distended with perfluorocarbon (3 mol/L-Fluorinert, 3M, St. Paul, Minnesota) to a volume of approximately 50 ml to reduce susceptibility artifacts induced by air in the coil's balloon. The MRI protocol included triplanar T2W turbo spin echo, DW MRI, 3D MR point resolved spectroscopy, axial pre-contrast T1-weighted axial 3D fast field echo DCE MRI sequences, and their detailed sequence parameters were defined in a prior study.[12] The mean interval between MRI and radical prostatectomy was 60 days (range 3 to 180, median 48). The interval between TRUS guided biopsy and MRI was 10 or more weeks to avoid post-biopsy hemorrhage related MRI signal changes.

Preparation of Customized MRI Based Mold

Following MRI, 3D models of each prostate were generated using ANALYZE software (Mayo Clinics, Analyze-Direct, Inc., Overland Park, Kansas). Generation of the 3D model included segmentation of the prostate capsule on in vivo triplane T2W MRI, fusion of the binary objects, and surface extraction of high resolution 3D surfaces from the binary object. Each mold was designed using commercially available 3D computer aided design software (Solidworks, Dassault Systèmes SolidWorks Corp., Concord, Massachusetts) and the design incorporated the deformation of the endorectal coil. A 3D printer (Dimension Elite 3D printer, Stratasys, Inc., Eden Prairie, Minnesota) which prints by depositing acrylonitrile butadiene styrene plastic was used to fabricate each mold (fig. 1). Following robotic radical prostatectomy the specimen was fixed in formalin for 2 to 24 hours at room temperature, then seminal vesicles were amputated and the specimen was placed in the customized 3D mold and sliced in axial 6 mm sections.[18] This short period of fixation makes the specimen firm and allows slicing without distortion.

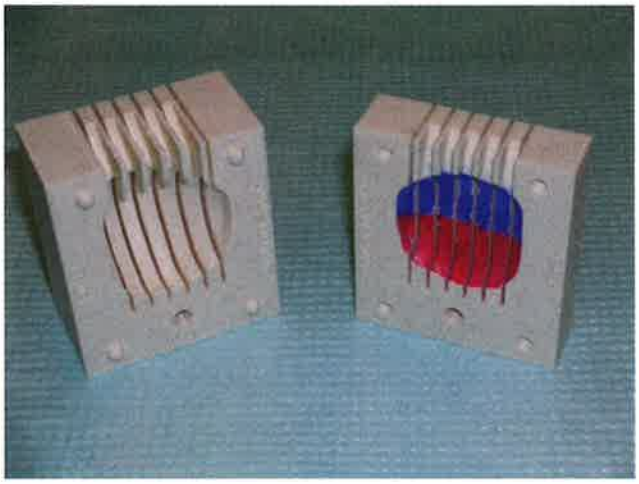

Figure 1. Customized MRI based prostatectomy mold

MRI and Histopathological Analysis

Tumors were mapped prospectively on multiparametric MRI (each MRI sequence was evaluated separately and independently) by 2 radiologists (BT, PLC) with an accumulated experience of prostate MRI of 4 and 12 years, respectively. MRIs were assessed in consensus. Although both reviewers were aware that patients had biopsy proven prostate cancer, they were blinded to preimaging serum PSA, TRUS guided biopsy results and histopathology findings. Whole mount histopathol- ogy specimens sectioned in the customized mold were mapped for individual tumor foci, dimensions and Gleason scores independently by 2 experienced pathologists (HM, MJM) blinded to MRI. For tumor localization on MRI and histopathology, the prostate gland was divided into axial sections (the number of axial sections varied between 4 and 7 depending on the dimension of the prostatectomy specimen). Sectioning of the gross specimen in the molds corresponded to the axial plane of the MRI sections. These whole mount sections were processed for histopathology, and paraffin embedded sections were evaluated for the presence and grade of cancer. Foci of cancer were marked on each slide with 2-axis measurements in millimeters. These foci were then mapped on paper. For comparative evaluation each of the slices was divided on paper into 6 regions, including 4 PZ sections (right anterior, right posterior, left anterior, left posterior) and 2 CG regions (right, left). Thus, all histology sections were annotated.

MRI and Histopathology Correlation

The customized mold provided whole mount tissue blocks that have one-to-one correspondence to the in vivo MRI. The annotated histology images of each whole mount specimen were stringently correlated with the corresponding slice of the multiparametric MRI (fig. 2). For region based correlation, the annotated histology region and corresponding MRI having marked tumors were simultaneously displayed on computer using MIPAV (http://mipav.cit.nih.gov/) software and no correction or approximation was performed during correlation.

Statistical Analysis

Statistical analysis was performed to assess the correlation between MRI and histopathology. Sensitivity, specificity, PPVs and NPVs of MRI were calculated in the PZ, CG, anterior peripheral zone (including the anterior stroma, bilateral A&CG) and in the overall prostate gland. MRI sequence sensitivity was defined as the probability of correctly identifying a histopathologically proven tumor focus in a given region. Specificity was defined as the probability of correctly identifying regions negative for tumor. Estimates of sensitivity and specificity were obtained by first estimating the sensitivity and specificity across all levels of zones of interest for each patient. Sensitivity and specificity were then estimated by averaging the individual specific estimates across patients. The variance of the estimate is the sample variance divided by the number of patients. We tested for differences in sensitivity and specificity between different modalities by testing for differences in individual specific estimates using the paired Wilcoxon rank test.

We then analyzed the effect of histopathological variables on the sensitivity of each MRI sequence accounting for the correlation among the multiple regions on the same patient. Specifically we evaluated the effect of lesion size (greatest diameter 5 mm or less vs more than 5 mm) and Gleason score (7 or less vs greater than 7) for each tumor focus in 4 different zones. GEEs with logit link and working independence correlation structure were used to estimate sensitivity and to test the effect of histopathological variables on sensitivity. GEEs were also used to evaluate the combined diagnostic accuracy of multiple MRI variables in a region on the probability of cancer within that region. Robust variance estimate and delta method were used to calculate the standard errors of PPV. Eleven GEE models with different combinations of MRI sequences were fitted for each zone and each modality. The Wald test with robust variance estimate was used for inference. All p values correspond to 2-sided tests with $p < 0.05$ considered statistically significant.

RESULTS

Histopathological Findings

Whole mount histopathological evaluation of 45 prostatectomy specimens revealed 342 tumor positive regions (281 [82%] in PZ and 61 [18%] in CG) among 1,746 regions. Of these 342 tumor positive regions, 110 (90 [82%] in PZ and 20 [18%] in CG) contained tumors 5 mm or less in diameter, whereas 232 (191 [82%] in PZ and 41 [18%] in CG) contained tumors greater than 5 mm in diameter. Gleason scores were 7 or less in 235 (194 [82.5%] in PZ and 41 [17.5%] in CG) regions and greater than 7 in 107 (87 [81%] in PZ and 20 [19%] in CG) regions. On histopathological evaluation extracapsular extension was detected in 20 regions in 12 prostatectomy specimens. Seminal vesicle invasion was detected in 2 patients.

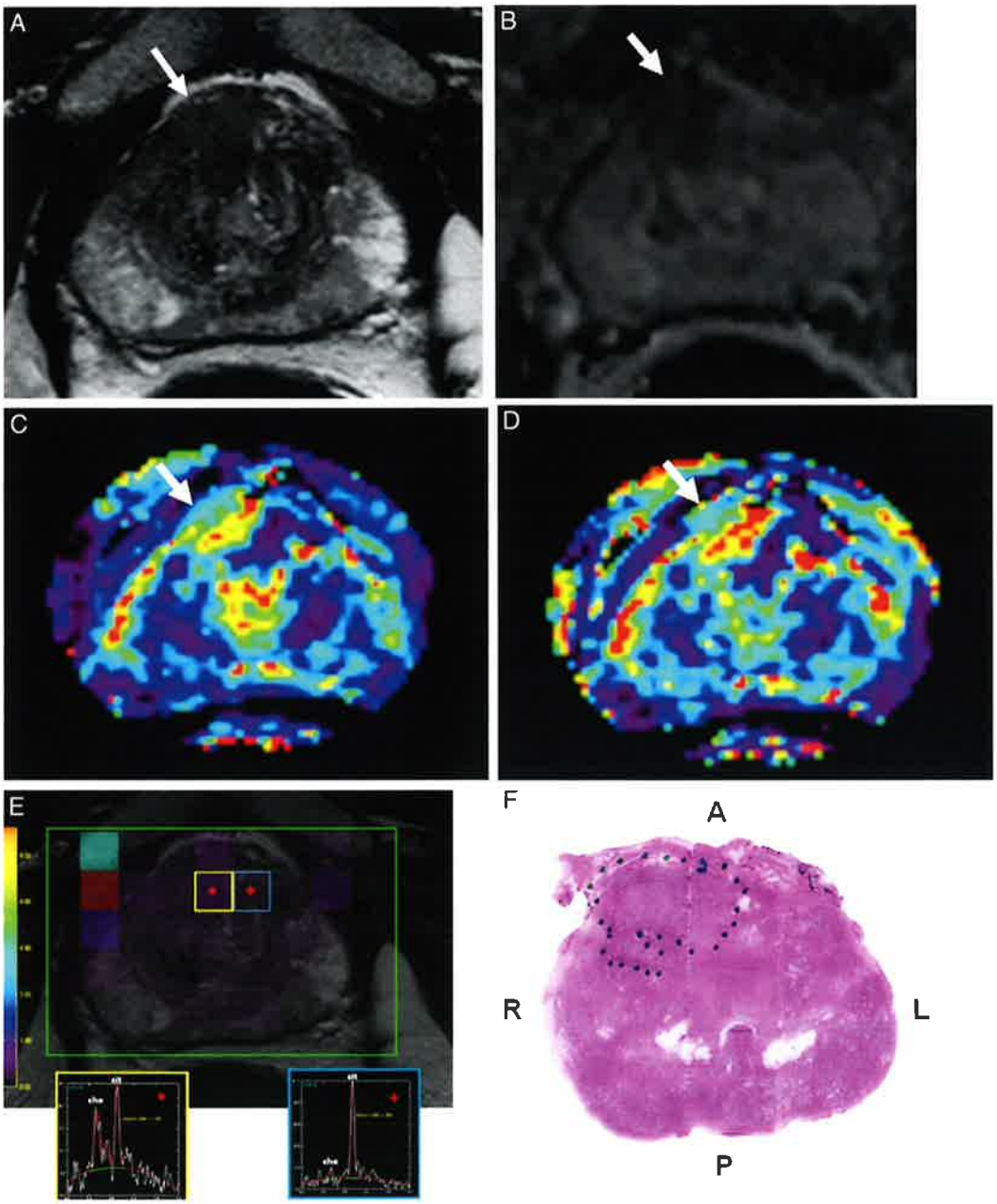

Figure 2. Prostate cancer in 52-year-old man. Axial T2-weighted and ADC map (*A*) of diffusion weighted (*B*) MRI demonstrates low signal intensity lesion (arrows) in right mid anterior central gland lesion suspicious for cancer. K^{trans} (*C*) and k_{ep} (*D*) maps of dynamic contrast enhanced MRI localize tumor (arrows). MRS (*E*) demonstrates increased ratio of choline (*cho*)-to-citrate (*cit*) in right mid anterior central gland lesion (asterisk) compared with normal adjacent left side (plus sign). Histopathological slide (*F*) at mid prostate level confirms presence of tumor (Gleason score 7, broken line) detected on multiparametric MRI. *A*, anterior. *L*, left. *P*, posterior. *R*, right. Reduced from x100.

MRI Findings

Based on the results of the GEEs/logistic regression, all 4 MRI combined sequences provided significant improvement in positive predictive value compared to each single MRI sequence and some doublet MRI sequences ($p < 0.01$). For example, in the peripheral zone the PPV estimated from the GEE using all 4 MRI sequences was 98%, which was significantly higher than using T2W MRI alone (PPV 69%), and using a combination of T2W MRI and ADC maps of DW MRI. In the central gland the PPV using all 4 MRI sequences was 97% vs 87% using T2W MRI alone. Tables 1 and 2 summarize the individual sensitivity, specificity, and positive and negative predictive values of the 4 MRI sequences for the PZ, CG, A&CG and overall prostate gland. The sensitivity for T2W MRI and ADC maps of DW MRI was significantly higher than MRS and DCE MRI in the PZ

Table 1. *Sensitivity and specificity for each MRI sequence in different prostate zones*

	PZ	CG	A&CG	Overall Gland
% Sensitivity (p value):				
T2W	0.65 (0.04)	0.15 (0.08)	0.38 (0.07)	0.58 (0.04)
ADC	0.57 (0.04)	0.22 (0.09)	0.44 (0.07)	0.53 (0.04)
MRS	0.17 (0.04)	0.08 (0.06)	0.15 (0.05)	0.16 (0.04)
DCE	0.39 (0.05)	0.22 (0.09)	0.31 (0.07)	0.38 (0.05)
% Specificity (p value):				
T2W	0.9 (0.02)	1 (0)	0.98 (0.01)	0.93 (0.01)
ADC	0.93 (0.02)	0.97 (0.01)	0.97 (0.01)	0.95 (0.01)
MRS	1 (0)	1 (0)	1 (0)	1 (0)
DCE	0.97 (0.01)	0.99 (0)	0.99 (0)	0.98 (0.01)

In peripheral zone and overall gland, except for the comparisons between T2W MRI and ADC maps of DW MRI, the 4 modalities had significantly different sensitivity and specificity ($p < 0.01$), with T2W having the highest sensitivity and MRS having the highest specificity. In the central gland most of the differences in sensitivity and specificity were not significant. In the anterior peripheral zone and central gland, T2W MRI, ADC maps of DW MRI and DCE MRI had significantly higher sensitivity than MRS ($p < 0.01$).

as well as in the overall prostate gland ($p < 0.01$ for all pair-wise comparisons), whereas for the CG and A&CG regions T2W MRI, ADC maps of DW MRI and DCE MRI had significantly higher sensitivity than MRS ($p < 0.01$). Positive predictive values of T2W MRI, ADC maps of DW MRI, MRS and DCE MRI were 0.7, 0.73, 0.93 and 0.86, respectively, in the overall prostate gland ($p < 0.01$), and NPVs of each MRI sequence were similar (table 2). The results presented in table 3 suggest that sensitivity increases with the lesion size and Gleason score. With the exception of MRS in the PZ and overall prostate gland, sensitivity was higher for tumors larger than 5 mm in diameter vs 5 mm or less. Sensitivity improved for tumors with higher Gleason scores (greater than 7) in each modality in all prostate zones ($p < 0.01$).

On MRI the region analysis revealed extracapsular extension in 27 regions in 18 patients, which included possible multiple regions from the same patient. That analysis revealed sensitivity and specificity rates of 85% and 99%, respectively. However, on a per patient analysis predicting extracapsular extension the sensitivity and specificity rates decreased to 78% and 79%, respectively.

DISCUSSION

An ancillary benefit of MRI is that it may more accurately stage tumors before treatment. This technology will potentially be useful in image guided, focal therapy as well as whole gland therapy such as surgery or radiation. Our data indicate that multiparametric prostate MRI at 3T enables accurate tumor detection with reasonable sensitivity and specificity. Among the MRI sequences, T2W MRI, ADC maps of DW MRI and DCE MRI were the most helpful for tumor detection in the central gland, where a significant overlap between tumors and benign prostatic hyperplastic changes usually occurs. A combination of DW MRI and DCE MRI demonstrated the most promising sensitivity for anterior PZ and CG tumors. Traditionally, systemic TRUS guided biopsy under samples the CG and the anterior PZ.

MRI has better sensitivity for detecting larger (more than 5 mm in diameter) and more aggressive (Gleason score greater than 7) tumors, indicating that it may preferentially detect clinically relevant tumors.[19] In addition, for overall prostate cancer detection, multiparametric MRI performed better than any individual MRI sequence. The improved value of sequential MRI at 3T which includes T2W MRI, ADC maps of DW MRI, choline-to-citrate ratio of MRS and permeability parameters derived from DCE MRI, is demonstrated in this data.

The customized mold provided tissue blocks that permitted a direct one-to-one correlation with in vivo MRI. The use of the customized mold enabled more exact correlation between each MRI parameter and the histopathological specimen, without requiring a correction or an approximation approach. In prior studies to correct the mismatches between MRI and histopathology several methods have been proposed. Scheidler et al used a methodology which considered tumor sites detected on MRI and histopathology if they were in the same sextant within a range of 1 section (±3 to 4 mm craniocaudally) provided that they were in the same anterior or posterior prostatic hemisphere.[16] Villers et al matched MRI with histopathology based on anatomical landmarks such as gland contours.[17] Other groups accepted a distance of 8 to 10 mm (approximately 2 sections) as evidence of a match between MRI and histopathology.[9,20,21] Before the current specimen mold technique, a nearest neighbor approach had been used by our group to validate MRI with a more standardized, unbiased method.[12] Moreover, the ma-

Table 2. *Positive and negative predictive values for each MRI sequence in different prostate zones*

	PZ	CG	A&CG	Overall Gland
% PPV (p value):				
T2W	0.69 (0.05)	0.87 (0.1)	0.73 (0.09)	0.7 (0.05)
ADC	0.74 (0.04)	0.63 (0.13)	0.75 (0.06)	0.73 (0.04)
MRS	0.94 (0.04)	0.89 (0.1)	0.96 (0.04)	0.93 (0.04)
DCE	0.86 (0.05)	0.86 (0.07)	0.89 (0.04)	0.86 (0.04)
% NPV (p value):				
T2W	0.89 (0.02)	0.92 (0.02)	0.93 (0.01)	0.9 (0.01)
ADC	0.87 (0.02)	0.92 (0.02)	0.94 (0.01)	0.89 (0.01)
MRS	0.8 (0.02)	0.91 (0.02)	0.91 (0.01)	0.83 (0.01)
DCE	0.84 (0.02)	0.92 (0.02)	0.92 (0.01)	0.87 (0.01)

PPVs were significantly different among the 4 MRI sequences ($p < 0.01$) whereas NPVs were similar.

Table 3. *Effects of tumor characteristics on sensitivity of each MRI sequence in different prostate zones*

	T2W MRI % Sensitivity (p value)	DCE MRI % Sensitivity (p value)	MRS % Sensitivity (p value)	DW MRI % Sensitivity (p value)
Overall prostate gland:				
Gleason score 7 or less	0.47 (0.05)	0.27 (0.05)	0.14 (0.04)	0.45 (0.05)
Gleason score greater than 7	0.8 (0.06)	0.69 (0.08)	0.32 (0.14)	0.74 (0.07)
Size 5 mm or less	0.37 (0.05)	0.13 (0.03)	0.08 (0.03)	0.33 (0.06)
Size greater than 5 mm	0.68 (0.05)	0.53 (0.07)	0.25 (0.08)	0.64 (0.06)
Peripheral zone:				
Gleason score 7 or less	0.56 (0.05)	0.30 (0.05)	0.17 (0.04)	0.52 (0.06)
Gleason score greater than 7	0.85 (0.05)	0.69 (0.09)	0.30 (0.17)	0.74 (0.08)
Size 5 mm or less	0.45 (0.05)	0.15 (0.04)	0.10 (0.04)	0.40 (0.07)
Size greater than 5 mm	0.75 (0.05)	0.55 (0.07)	0.26 (0.09)	0.68 (0.06)
Central gland:				
Gleason score 7 or less	0.05 (0.05)	0.12 (0.08)	0 (0)	0.10 (0.07)
Gleason score greater than 7	0.6 (0.21)	0.7 (0.18)	0.4 (0.23)	0.75 (0.18)
Size 5 mm or less	0 (0)	0.05 (0.05)	0 (0)	0 (0)
Size greater than 5 mm	0.34 (0.15)	0.44 (0.14)	0.2 (0.13)	0.46 (0.16)
A&CG:				
Gleason score 7 or less	0.29 (0.07)	0.18 (0.06)	0.06 (0.03)	0.35 (0.07)
Gleason score greater than 7	0.76 (0.13)	0.79 (0.12)	0.5 (0.18)	0.84 (0.11)
Size 5 mm or less	0.12 (0.07)	0.07 (0.04)	0.02 (0.02)	0.29 (0.1)
Size greater than 5 mm	0.57 (0.09)	0.49 (0.1)	0.27 (0.11)	0.59 (0.09)

With the exception of MRS in the PZ and overall prostate gland, all 4 MRI sequences had significantly higher sensitivity in detecting larger tumors and tumors with Gleason score greater than 7 ($p < 0.05$ for all comparisons).

jority of the studies correlating MRI with histopathology do not directly acknowledge the difficulties in matching imaging to histopathology. The use of a customized specimen mold in this study allowed us to better validate MRI in prostate cancer detection and localization, and helped us to improve our results in terms of tumor detection and local staging at MRI compared to our prior correlation results.[12]

Our study has several limitations. The radiologists reviewing the MRI knew that all patients included in the study had biopsy proven cancer and this could lead to bias during the interpretation of the magnetic resonance images. In addition, the customized MRI based specimen mold is relatively expensive. Therefore, we do not advocate it for routine clinical use. However, such a systematic method can be useful in multicenter clinical trials. It was used for research purposes only in this study. Finally, we sliced the prostate in 6 mm sections, whereas the MRI was obtained in 3 mm slice thicknesses. In future studies we intend to slice the sections at 3 mm intervals.

CONCLUSIONS

Prostate MRI at 3T allows for the detection of prostate cancer. In particular, a multiparametric approach increases the predictive power of MRI for diagnosis. The patient specific mold provides evenly spaced tissue blocks of uniform thickness which correspond directly to the MRI slice planes, leading to improved co-registration with histology compared with prior freehand methods. MRI may provide the urologist an imaging modality to better treat patients with prostate cancer. With continued research this imaging platform may also allow a more accurate method for cancer detection than traditional systematic nonguided biopsies. Compared to the traditional biopsy method, multiparametric imaging may allow earlier diagnosis of anterior prostate lesions and can guide needle biopsies more accurately than systematic methods. These findings may also provide the basis for image guided, minimally invasive, focal treatments of prostate cancer.

REFERENCES

1. American Cancer Society: Cancer Facts & Figures 2010. Atlanta: American Cancer Society 2010.
2. Kim CK, Park BK and Kim B: Localization of prostate cancer using 3T MRI: comparison of T2-weighted and dynamic contrast-enhanced imaging. J Comput Assist Tomogr 2006; **30:** 7.
3. Torricelli P, Cinquantini F, Ligabue G et al: Comparative evaluation between external phased array coil at 3 T and endorectal coil at 1.5 T: preliminary results. J Comput Assist Tomogr 2006; **30:** 355.
4. Park BK, Kim B, Kim CK et al: Comparison of phased-array 3.0-T and endorectal 1.5-T magnetic resonance imaging in the evaluation of local staging accuracy for prostate cancer. J Comput Assist Tomogr 2007; **31:** 534.
5. Fütterer JJ, Heijmink SW, Scheenen TW et al: Prostate cancer localization with dynamic contrast-enhanced MR imaging and proton MR spectroscopic imaging. Radiology 2006; **241:** 449.

6. Kim CK, Park BK, Lee HM et al: Value of diffusion-weighted imaging for the prediction of prostate cancer location at 3T using a phased-array coil: preliminary results. Invest Radiol 2007; **42:** 842.

7. Ocak I, Bernardo M, Metzger G et al: Dynamic contrast-enhanced MRI of prostate cancer at 3 T: a study of pharmacokinetic parameters. AJR Am J Roentgenol 2007; **189:** 849.

8. Scheenen TW, Heijmink SW, Roell SA et al: Three-dimensional proton MR spectroscopy of human prostate at 3 T without endorectal coil: feasibility. Radiology 2007; **245:** 507.

9. Heijmink SW, Fütterer JJ, Hambrock T et al: Prostate cancer: body-array versus endorectal coil MR imaging at 3 T–comparison of image quality, localization, and staging performance. Radiology 2007; **244:** 184.

10. Miao H, Fukatsu H and Ishigaki T: Prostate cancer detection with 3-T MRI: comparison of diffusion-weighted and T2-weighted imaging. Eur J Radiol 2007; **61:** 297.

11. Zhang J, Hricak H, Shukla-Dave A et al: Clinical stage T1c prostate cancer: evaluation with endorectal MR imaging and MR spectroscopic imaging. Radiology 2009; **253:** 425.

12. Turkbey B, Pinto P, Mani H et al: Prostate cancer: value of multiparametric MR imaging at 3 T for detection– histopathologic correlation. Radiology 2010; **255:** 89.

13. Rosenkrantz AB, Neil J, Kong X et al: Prostate cancer: comparison of 3D T2-weighted with conventional 2D T2-weighted imaging for image quality and tumor detection. AJR Am J Roentgenol 2010; **194:** 446.

14. Riches SF, Payne GS, Morgan VA et al: MRI in the detection of prostate cancer: combined apparent diffusion coefficient, metabolite ratio, and vascular parameters. AJR Am J Roentgenol 2009; **193:** 1583.

15. Kitajima K, Kaji Y, Fukabori Y et al: Prostate cancer detection with 3 T MRI: comparison of diffusion-weighted imaging and dynamic contrast-enhanced MRI in combination with T2-weighted imaging. J Magn Reson Imaging 2010; **31:** 625.

16. Scheidler J, Hricak H, Vigneron DB et al: Prostate cancer: localization with three-dimensional proton MR spectroscopic imaging–clinicopathologic study. Radiology 1999; **213:** 473.

17. Villers A, Puech P, Mouton D et al: Dynamic contrast enhanced, pelvic phased array magnetic resonance imaging of localized prostate cancer for predicting tumor volume: correlation with radical prostatectomy findings. J Urol 2006; **176:** 2432

18. Shah V, Pohida T, Turkbey B et al: A method for correlating in vivo prostate magnetic resonance imaging and histopathology using individualized magnetic resonance-based molds. Rev Sci Instrum 2009; **80:** 104301.

19. Turkbey B, Albert PS, Kurdziel K et al: Imaging localized prostate cancer: current approaches and new developments. AJR Am J Roentgenol 2009; **192:** 1471.

20. Fütterer JJ, Engelbrecht MR, Huisman HJ et al: Staging prostate cancer with dynamic contrast-enhanced endorectal MR imaging prior to radical prostatectomy: experienced versus less experienced readers. Radiology 2005; **237:** 541.

21. Fütterer JJ, Heijmink SW, Scheenen TW et al: Prostate cancery: local staging at 3-T endorectal MR imaging–early experience. Radiology 2006; **238:** 184.